JOURNAL OF SPACECRAFT AND ROCKETS
Vol. 45, No. 4, July–August 2008

Engineering Model of Temperature-Induced Pneumatic Sensor Pressure Gradients for Rarefied Flow Conditions

Stephen A. Whitmore*
Utah State University, Logan, Utah 84322-4130

DOI: 10.2514/1.35277

An engineering model for calculating the rarefied flow-induced dc pressure offsets in pneumatic sensors is presented. At rarefied pressure levels, a low molecular density allows the fluid to "slip" at solid boundaries. Under rarefied flow conditions in which the pressure tube is heated unevenly, the wall slip allows the hot end of the tube to have a higher pressure than the cold end of the tube with no net flow. This thermomolecular effect results in a bias in the sensed pressure. An existing model, derived from fluid dynamic analysis with a slip-flow wall boundary condition, accurately predicts the induced dc pressure bias up to approximately 0.7 Knudsen number. A more extensive engineering model is derived in this paper. This engineering model is a curve fit of empirical data and predicts the slip-induced pressure gradients for the range of Knudsen numbers from continuum to free molecular flow. Five degrees of freedom are necessary to fit the data with acceptable accuracy. The model parameters were calculated using a nonlinear regression algorithm. An example calculation for a flush air-data sensing system on a reentry capsule is presented. When the surface Knudsen number for one of the ports in the windward/leeward pressure pair rises above approximately 0.1, that pair is no longer usable.

Nomenclature

a	=	curve-fit parameter
b	=	curve-fit parameter
c	=	curve-fit parameter
D	=	tube diameter, cm
d	=	curve-fit parameter
dP/P	=	normalized pressure gradient along pneumatic tubing
dT/T	=	normalized temperature gradient along pneumatic tubing
e	=	curve-fit parameter
i	=	longitudinal reentry flush air-data sensing pressure station index
L	=	pneumatic tubing length, m
P	=	generic pressure symbol, kPa
P_{cold}	=	pressure at cold end of tube, kPa
P_{hot}	=	pressure at hot end of tube, kPa
P_{leeward}	=	pressure on leeward surface of spacecraft, kPa
P_{sensed}	=	pressure as sensed by transducer, kPa
P_{surface}	=	pressure at spacecraft surface, kPa
P_{windward}	=	pressure on windward surface of spacecraft, kPa
R_g	=	gas constant for air, 287.1 J/kg-K
T	=	temperature, K
T_{cold}	=	temperature at cold end of pneumatic tube, K
T_{hot}	=	temperature at hot end of pneumatic tube, K
V	=	entrapped volume of pressure sensor, cm^3
X	=	longitudinal coordinate, m
Z	=	normal coordinate, m
α	=	angle of attack, deg
ΔP	=	pressure error, $P_{\text{surface}} - P_{\text{sensed}}$, kPa.
ε	=	ratio of slip distance to mean free path
κ_n	=	Knudsen number
μ	=	dynamic viscosity, $Nt \cdot \text{s/m}^2$
μ_{mean}	=	mean error in curve fit
σ_{rms}	=	root mean square error in curve fit

Received 23 October 2007; revision received 27 March 2008; accepted for publication 28 March 2008.

*Assistant Professor, Mechanical and Aerospace Engineering Department, 4130 Old Main Hill/UMC 4130. Associate Fellow AIAA.

I. Introduction

MEASURING surface pressures on hypersonic vehicles presents a formidable challenge. The hostility of the sensing environment precludes intrusion into the flow, and measurements must be obtained using significant lengths of pneumatic tubing to connect the surface ports to remotely located pressure transducers. An idealized pressure sensor is depicted in Fig. 1. In this sensor model, a small volume is attached to the downstream end of the pressure tube to represent the entrapped volume of a pressure transducer and fitting. Pressure impulses at the surface are transmitted as longitudinal waves, and the pressure tubing has the effect of damping and delaying the sensed pressure signal. Problems associated with predicting tube flow dynamics have been studied extensively. The methods of Berg and Tijdeman [1] are currently considered the state of the art for the calculation of pneumatic responses for cascaded geometries with constant wall temperatures and continuum flow.

In hypersonic flow regimes, the associated surface heating results in large temperature gradients along the length of the pneumatic tubing. Additionally, high surface temperatures mandate that the surface ports and pneumatic tubing be small to avoid hot ingestion. As a final complication, when one moves away from the stagnation region, the surface pressure levels drop rapidly. This combination of very low pressure levels, small diameter pneumatic lines, and large temperature gradients produce some unusual effects in pneumatic sensor configurations for hypersonic flight conditions. To obtain accurate measurements, the effects of low Knudsen number flow conditions must be accounted for in the pressure sensing system design. For the purposes of this discussion, fluid flow regimes are classified as *continuum*, *slip flow*, and *free molecular flow*. Continuum flow occurs for Knudsen numbers below 0.01 and is characterized by the classical "no-slip" boundary condition along the solid surfaces. The slip-flow regime occurs for Knudsen numbers between 0.01 and 1.0 and is characterized by very low pressure levels. In the slip-flow regime, the fluid flow away from the solid boundaries is identical to continuum flow but, at the surface, fluid particles no longer "stick" to the surface but slide along the boundary. Slip-flow conditions can be analyzed using the equations of fluid dynamics with a modified set of surface boundary conditions. Free molecular flow occurs at Knudsen numbers above 1.0 and, for these conditions, one must resort to statistical thermodynamics to model

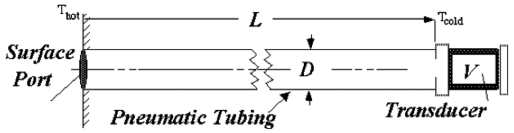

Fig. 1 Schematic of the idealized pressure sensor configuration.

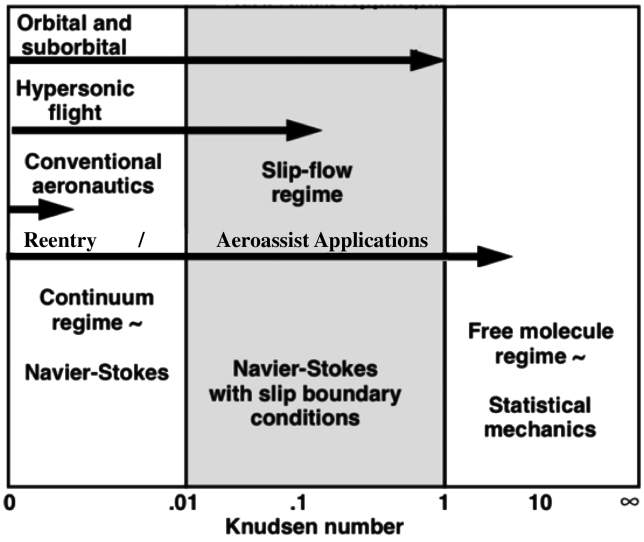

Fig. 2 Flight applications and Knudsen number ranges for continuum, slip-flow, and molecular flow regimes.

the fluid behavior. Both slip flow and free molecular flow are referred to as "*rarefied*" conditions. Figure 2 shows some typical flight applications and the corresponding fluid dynamic flow regimes.

II. Practical Knudsen Number Definition

The Knudsen number [2] is the most import nondimensional parameter used to classify rarefied gas phenomena. Strictly speaking, the Knudsen number is defined as the ratio of the average distance that each fluid particle travels between collisions (the mean free path distance) and the characteristic length scale of the system. If the length scale of the system is defined as half of the tube diameter, the Knudsen number can be approximated by the expression

$$\kappa_n = \frac{2\mu}{D \cdot P}\sqrt{R_g \pi \cdot T} \tag{1}$$

This definition is convenient for the purposes of this discussion in that it allows the rarefied flow effects to be characterized by two directly sensible parameters: pressure and temperature.

III. Rarefied Flow Effects on Pressure Measurements at High Knudsen Numbers

For typical continuum flow measurement applications, pressure sensor pneumatic components only affect the dynamic response of the system. The dc signal component of the incoming pressure signal is unaltered. This constant dc pressure result is no longer true under rarefied flow conditions in which fluid slips at the tube wall boundary. When the tube is heated unevenly, as is the case when pressures are being sensed on a hot surface, the wall slip manifests itself as a dc offset in the measured pressure reading. This *thermomolecular effect* is a peculiar phenomenon that occurs at low pressures. For rarefied flow conditions, the fluid velocity at the wall can be decomposed into two parts [3]: the wall *slip velocity* and the *thermomolecular "creep" velocity*. The wall slip velocity is a result of reduced bulk fluid viscosity under rarefied flow conditions. The thermomolecular creep is a transpiration phenomenon and is described by statistical thermodynamics. Along an unequally heated gas boundary, Maxwell's kinetic theory [4] predicts that gas molecules originating in the hot region of the tube have a higher kinetic energy than molecules originating from the cold region. As a result, these hot molecules recoil more strongly than molecules from the cold side of the tube. The net result is that the gas acquires a longitudinal momentum in the hotter direction. The net momentum gain causes gas molecules at the wall to creep from the cold end of the tube to the hot end of the tube. To balance this creep, the gas molecules in the center of the tube migrate toward the colder end of the tube. This opposing flow equilibrium results in a steady-state pressure gradient with the cold region of the tube having a lower pressure than the hot region and no net cross-sectional flow in the tube.

A. Free Molecular Flow Conditions

Maxwell determined that in free molecular flow the normalized ratio of the rarefied flow-induced pressure gradient equals one-half of the normalized temperature gradient:

$$\frac{\mathrm{d}P/P}{\mathrm{d}T/T} \approx \frac{P_{\text{hot}} - P_{\text{cold}}}{\frac{1}{2}(P_{\text{hot}} + P_{\text{cold}})} \Big/ \frac{(T_{\text{hot}} - T_{\text{cold}})}{\frac{1}{2}(T_{\text{hot}} + T_{\text{cold}})} = \frac{1}{2} \tag{2}$$

Maxwell's analysis was based only on molecular flow to which the equations of fluid mechanics no longer apply, and Eq. (1) can be considered as strictly valid as the Knudsen number approaches infinity. For finite Knudsen numbers, the equations of fluid mechanics are still valid away from the wall boundary, and early experiments by Tompkins and Wheeler [5] showed that the induced pressure gradient is strongly a function of Knudsen number and the temperature gradient along the tube. Whitmore et al. later verified these results in a series of alternate experiments [6,7]

B. Slip-Flow Conditions

As mentioned earlier, slip-flow conditions correspond to flow regimes with Knudsen numbers between approximately 0.01 and 1.0. For these conditions, which lie somewhere between the continuum and free molecular regimes, the pressure gradient induced by the longitudinal temperature gradients is less than the limit predicted by Maxwell [Eq. (2)] and is strongly a function of the Knudsen number. Whitmore et al. [6,7] have shown that the steady-state pressure gradient for slip-flow conditions is approximated by

$$\frac{\mathrm{d}P/P}{\mathrm{d}T/T} = \frac{6\kappa_n^2}{\pi(1 + 4\varepsilon \cdot \kappa_n)} \tag{3}$$

Adapting the dynamic response model of Berg and Tijdeman [1] for a slip-wall boundary condition and then applying the final value theorem [8] to get steady-state conditions derived this result. Clearly, Eq. (3) does not approach an asymptotic limit for high Knudsen numbers and, thus, disagrees with the predictions of kinetic theory [Eq. (2)]. Furthermore, experimental observations in Whitmore et al. [6,7] show that the model of Eq. (3), although demonstrating excellent agreement at moderate Knudsen numbers, rapidly diverges from the experimental observations for $\kappa_n > 0.7$. Figure 3 presents this comparison. Clearly, a better engineering model is needed to allow for rarefied flow-induced pressure gradient predictions for the entire range of Knudsen numbers.

IV. Curve Fit of Experimental Data

Because of the asymptotic nature of the molecular flow effects at very low (continuum) and very high (*free molecular*) Knudsen numbers, simple polynomial curve fits are not acceptable for the data in Fig. 3. The fitting function must asymptotically approach zero at low Knudsen numbers while simultaneously approaching the free molecular limit of $1/2$ at high Knudsen numbers. After considerable trial and error, a function of the form

$$\frac{\mathrm{d}P/P}{\mathrm{d}T/T} = \frac{1}{2}\left(\frac{1}{d + \frac{a}{\kappa_n}[(1 + b/\kappa_n)/(1 + c/\kappa_n)]} + \frac{(d-1)}{e/\kappa_n + d}\right) \tag{4}$$

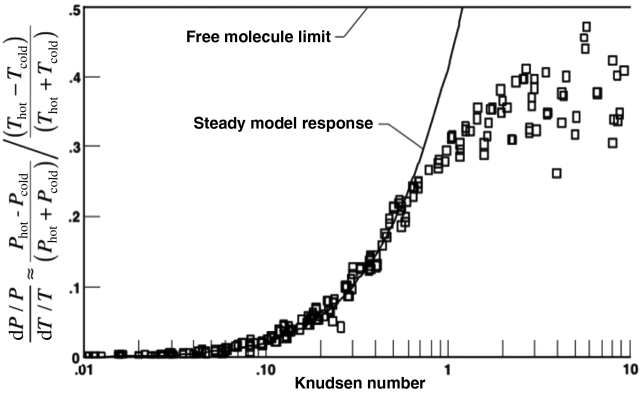

Fig. 3 Comparison of the steady-state slip-flow model pressure gradient parameter predictions to the measured data for rarefied flow conditions.

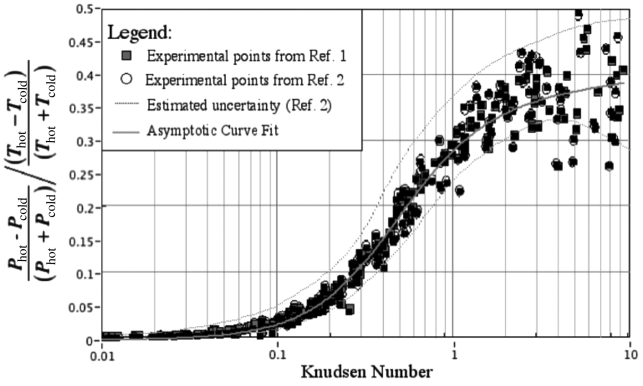

Fig. 4 Comparison of the empirical curve fit against the experimental data.

was found acceptable. Inspection reveals that this function shows the desired properties of having limiting values of zero at very small Knudsen numbers and of $1/2$ at very large Knudsen numbers. These limits are independent of the specific values that are chosen for the equation parameters. The parameters of the fit equation are evaluated by curve fitting the data of Eq. (3) using a nonlinear regression algorithm [9]. A total of five parameters (degrees of freedom) were necessary to match the inflections in the data curve and still allow for the required asymptotic behavior at low and high Knudsen numbers. To facilitate the regression analysis, Eq. (4) is rewritten in the more tractable analytical form:

$$\frac{\mathrm{d}P/P}{\mathrm{d}T/T} = \frac{1}{2}\left(\frac{d^2\cdot\kappa_n^3 + (a\cdot d + c\cdot d^2 + e - a)\kappa_n^2 + (c\cdot e + a\cdot b\cdot d - a\cdot b)\kappa_n}{d^2\cdot\kappa_n^3 + (a\cdot d + c\cdot d^2 + d\cdot e)\kappa_n^2 + (a\cdot b\cdot d + a\cdot e + c\cdot d\cdot e)\kappa_n + a\cdot b\cdot e}\right) \tag{5}$$

The regression analysis gives the minimum variance ("best fit") parameters as

$$\begin{bmatrix} a \\ b \\ c \\ d \\ e \end{bmatrix} = \begin{bmatrix} 0.194 \\ 1.399 \\ 0.048 \\ 1.310 \\ 100.000 \end{bmatrix} \tag{6}$$

The scatter in the data justifies only three significant digits for the curve-fit parameters. The resulting mean and root mean square errors for this curve fit are

$$\begin{bmatrix} \mu_{\text{mean}} = -0.000219 \\ \sigma_{\text{rms}} = 0.0432 \end{bmatrix} \tag{7}$$

Figure 4 shows the corresponding asymptotic curve fit overlaid onto the data along with the experimental uncertainty bounds calculated by Whitmore [7].

V. Application of Engineering Model to Reentry Flush Air-Data Sensing System

An example application for which the rarefied flow-induced dc offset of a sensed pressure can become significant is during planetary entry when pressure levels are low and surface temperatures are high. In this application, a reentry flush air-data sensing (RFADS) system [10,11] (flush surface pressure ports) is used to sense the atmospheric density and reentry angle of attack. These flow parameters are desirable for precise control of maneuvers including aerocapture, skip reentry, and aerobraking. For planetary entry, the spacecraft velocity can exceed 10 km/s, and the aerodynamic and radiative heating of the windward surfaces is generally extreme. For example, on lunar return trajectories both convective and radiative heating rates can exceed 200 W/cm^2 with a total heat load of more than 500 W/cm^2 near the stagnation point [12]. The hostility of the environment precludes placing ports on the windward surfaces, and pressure ports are placed away from the stagnation point in areas where the heating rates are less severe. This placement avoids problems with heating, but presents a potential problem with the very low pressure levels and large temperature gradients from the external ports to the sensing pressure transducers. The potential for rarefied flow-induced dc offsets in the pressure sensors is very high.

Figure 5 shows the flow pattern around and the pressure distribution along the centerline of an Orion-sized (Greathouse et al. [12]) capsule entering the Earth's atmosphere at Mach 20 and a 65-km altitude. Figure 5a shows the shock wave structure and external flow pattern at a 160-deg angle of attack (20 deg measured relative to the longitudinal centerline of the heat shield). The bow shock is extensively detached from the capsule and highly curved. The region behind the shock wave (with flow impinging on the heat shield) is subsonic and, as described earlier, the heating rates are very large. Figure 5b shows the pressure distribution along the lateral centerline of the vehicle at a 180-deg angle of attack (0 deg measured relative to the longitudinal centerline of the heat shield). As one "rounds the corner" away from the center of the heat shield, the flow rapidly accelerates and expands to supersonic conditions, and the pressure levels rapidly drop. The pressure is plotted on a logarithmic scale to clearly illustrate the very small pressures behind the heat shield shoulder. The calculations were performed using a commercially available computational fluid dynamics (CFD) code [13].[†] Less than 1 m aft of the leading edge of the heat shield, the pressures along the

[†]Data available online at Flow Modeling Solutions for the Aerospace & Defense Industries, Fluent, Inc., http://www.fluent.com/solutions/aerospace/index.htm [retrieved: 24 September 2007].

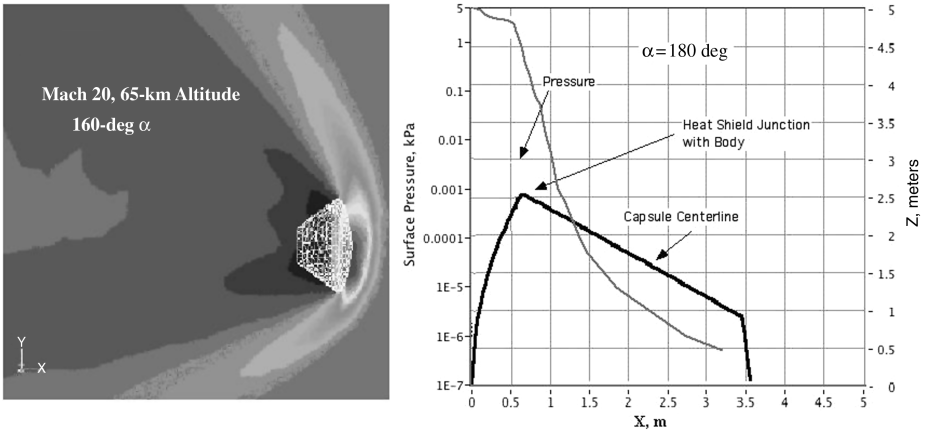

a) External flow pattern b) Lower centerline pressure distribution

Fig. 5 Reentry capsule bow shock wave structure and pressure distributions at Mach 20 and a 65-km altitude.

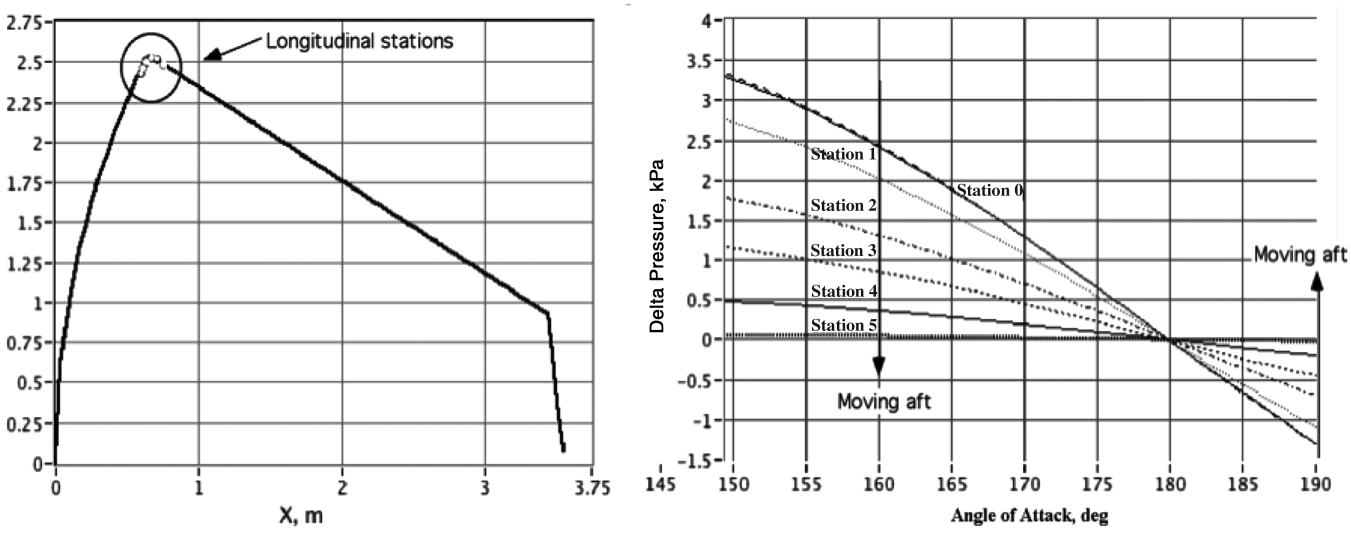

Fig. 6 Sensitivity of the windward and leeward surface pressure differences to the longitudinal stations and angle of attack.

surface of the body drop very quickly to less than the local ambient pressure level (0.0099 kPa).

Just aft of the heat shield junction with the conical afterbody, the pressures are extremely sensitive to the incoming flow direction, and this location offers a good choice for placing pressure ports to sense the vehicle angle of attack. Figure 6 demonstrates this sensitivity by plotting the differences between the windward and leeward centerline surface pressures as a function of the angle of attack at Mach 20 and a 65-km altitude. Figure 6a shows the locations of six longitudinal pressure stations along the shoulder and afterbody, and Fig. 6b plots the windward and leeward centerline pressure differences (calculated at the same longitudinal location) as a function of the freestream angle of attack. Table 1 lists the longitudinal (X) and normal (Z) coordinates for these port measurement station locations. The X coordinate is measured from the leading edge of the heat shield, and the Z coordinate is measured from the longitudinal centerline of the vehicle.

Table 1 Upper and lower surface measurement station coordinates

Upper (leeward) surface			Lower (windward) surface		
Station number	X, m	Z, m	Station number	X, m	Z, m
0	0.5625	2.4300	0	0.5625	−2.4300
1	0.5850	2.4700	1	0.5850	−2.4700
2	0.6025	2.4900	2	0.6025	−2.4900
3	0.6500	2.5350	3	0.6500	−2.5350
4	0.6925	2.5175	4	0.6925	−2.5175
5	0.7540	2.4800	5	0.7540	−2.4800

Depending on the shoulder radius of the curvature, the flow angle of attack, the local atmospheric density, the type of ablative material used, the wall catalycity, and the heat capacity of the wall itself, the temperatures at the heat shield shoulder can vary from approximately 1200 K on the leeward shoulder to more than to 3000 K (Greathouse et al. [12]) on the windward shoulder. The temperatures at these locations (Fig. 6) are low enough to allow port placement on the surface [14]; however, large temperature gradients along the pneumatic tubing from the port to the transducer will result. These temperature gradients coupled with low surface pressures have the potential to induce significant thermomolecular biases into the pressure readings. Equation (4) is used to calculate the thermomolecular measurement biases for each of the six longitudinal stations. To simplify the analysis, the temperatures of the windward and leeward shoulders are allowed to vary with the angle of attack, but the longitudinal temperatures are held constant for each of the measurement stations listed in Table 1. Figure 7 shows the upper and lower shoulder temperatures as a function of the angle of attack. Only angles of attack less than 180 deg (lift producing) are considered.

The viscosity is calculated as a function of the surface temperature using Sutherland's law [15] assuming nondissociated air and the standard value of 287.1 J/Kg · K for the specific gas constant. The transducers are assumed to be located within the body of the vehicle and maintained at a constant temperature of 50 C (323.15 K). The pressure tubing is assumed to be a constant 0.1-cm diameter from the surface port to the transducer. The formula of Eq. (2) is used to

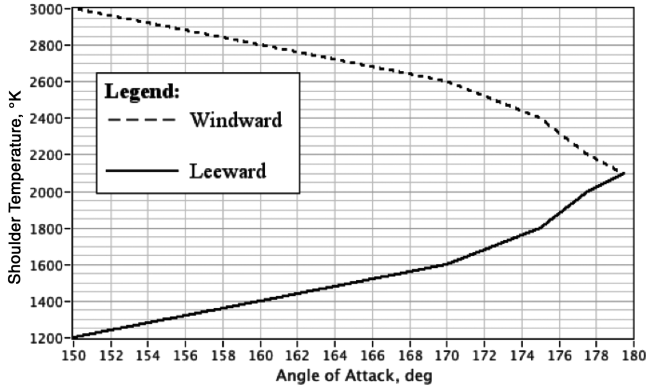

Fig. 7 Upper and lower heat shield shoulder temperatures.

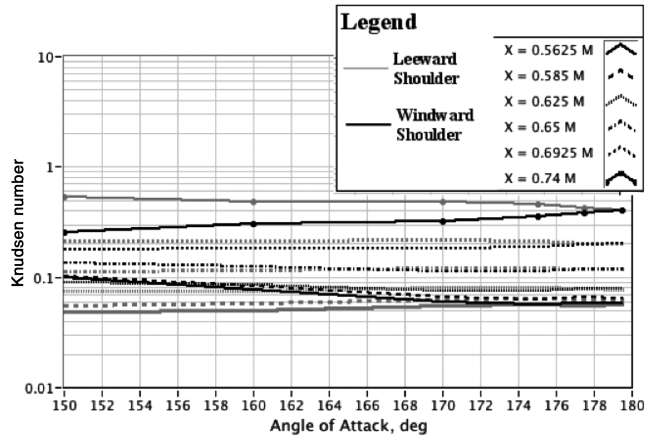

Fig. 8 Knudsen numbers for the upper and lower longitudinal stations, Mach 20, 65-km altitude.

calculate Knudsen numbers based on the local surface pressure. Figure 8 plots the resulting Knudsen numbers calculated using the pressure data in Figs. 5 and 6 and temperature data from Fig. 7. The calculated Knudsen numbers for both of the upper and lower shoulder measurement stations are plotted. The Knudsen numbers corresponding to the upper shoulder are plotted using gray lines, and the Knudsen numbers corresponding to the lower shoulder are plotted using black lines. The line styles for the longitudinal stations are indicated in the plot legend. The Knudsen numbers vary from less than 0.05 for the lower forward station to more than 0.5 for the aft upper station.

Using the temperatures assumed in Fig. 7, Eq. (4) is used to calculate the rarefied flow-induced pressure error in each of the 12 pressure readings. Figure 9 plots the resulting absolute pressure error

$$\Delta P = P_{\text{surface}} - P_{\text{sensed}}$$

for each of the 12 (six upper and six lower) measurement stations. The legend for this figure is the same as the legend for Fig. 8. Figure 10 plots the resulting normalized (percentage) error in the sensed pressure differential, that is, the difference between the sensed windward and leeward pressures when compared with the surface pressure differences for each of the six longitudinal station pairs (as plotted in Fig. 6),

$$\%\text{error}_i = \left[\frac{(P_{\text{windward}} - P_{\text{leeward}})_{\text{sensed}}}{(P_{\text{windward}} - P_{\text{leeward}})_{\text{surface}}}\right]_i \qquad i = 0, 2, \ldots, 5 \quad (8)$$

The percent errors (i.e., the normalized errors in the sensed differential pressure between the windward and leeward sides) in the sensed pressure pairs are a good indicator of the expected percentage errors in the angle of attack estimate. Thus assuming a 30-deg operating range for the system, the 1% differential pressure error in

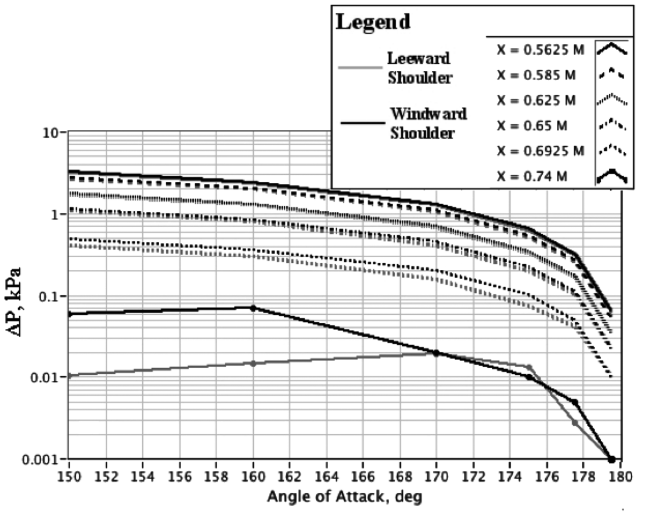

Fig. 9 Rarefied flow-induced pressure errors in RFADS, Mach 20, 65-km altitude.

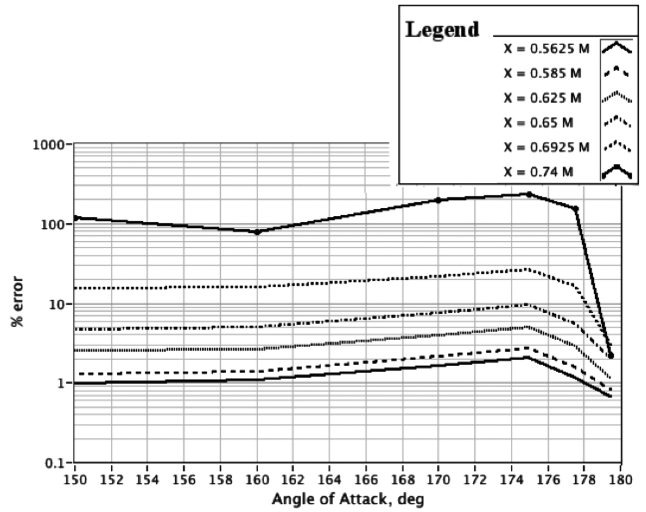

Fig. 10 Normalized error in the sensed windward/leeward pressure differential, Mach 20, 65-km altitude.

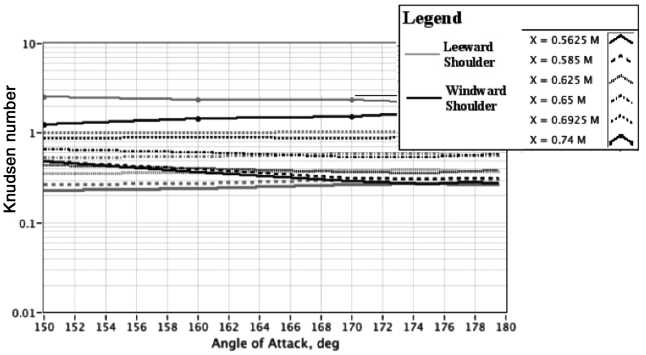

Fig. 11 Knudsen numbers for the upper and lower longitudinal stations, Mach 20, 75-km altitude.

the forward station pair results in a rarefied flow-induced angle of attack error of approximately 0.3 deg. The aft pressure pair results in a rarefied flow-induced angle of attack estimate of 300 deg and is totally unusable. In fact, only the forward two pairs have sufficiently low thermomolecular offsets to allow a usable angle of attack calculation.

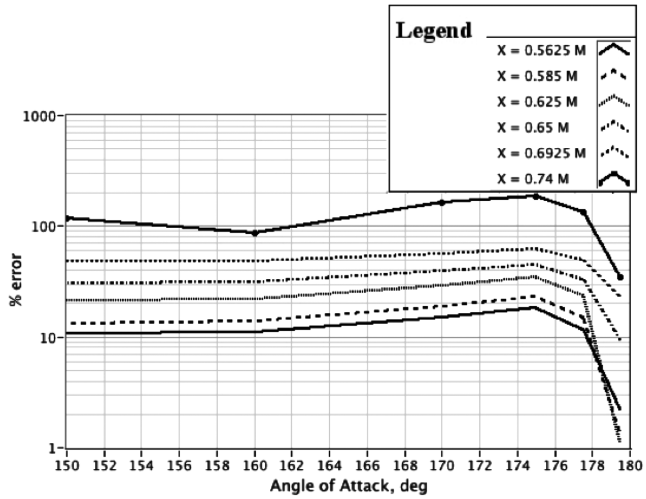

Fig. 12 Normalized error in the sensed windward/leeward pressure differential, Mach 20, 75-km altitude.

When the conditions examined in the previous example are allowed occur at a 10-km higher altitude (Mach 20 and a 75-km altitude), the resulting rarefied flow error renders the RFADS system unusable. These results are shown in Fig. 11 (Knudsen number) and Fig. 12 (% error). The higher altitude results in Knudsen numbers that are approximately an order of magnitude higher and produces ever larger thermomolecular effects.

It is conceivable that a "calibration" for these effects could be developed, but the best approach is to design the RFADS system so that it is insensitive to the rarefied flow-induced pressure errors. The curve fit depicted in Fig. 4 and the analysis presented in this section serve as guidance for this design process.

VI. Conclusions

The hostility of the sensing environment precludes intrusion into the flow, and measurements must be obtained using significant lengths of pneumatic tubing to connect the surface ports to remotely located pressure transducers. For typical measurement applications, the pressure tubing does not modify the dc component of the incoming pressure signal. This constant dc pressure result is no longer true under rarefied flow conditions in which the fluid slips at the tube wall boundary. When the tube is heated unevenly, as is the case when pressures are being sensed on a hot surface, the wall slip manifests itself as a dc offset in the measured pressure reading. This technical note curve fits the experimental data to give a unified model that predicts the rarefied flow-induced dc pressure gradient for all Knudsen numbers ranging from continuum to free molecular flow. After considerable trial and error, an acceptable function with the desired asymptotic properties was discovered. A total of 5 degrees of freedom were necessary to fit the data with an acceptable level of accuracy. An example calculation for a reentry air-data configuration was presented. CFD-derived pressure data are used to perform this analysis. Six longitudinal pressure pairs located on the windward and leeward shoulders of the reentry capsule were analyzed. These pairs are used to estimate the incoming flow angle of attack. The analysis shows that port placement is critical to eliminate potential dc offsets that will contaminate the angle of attack calculation. When the surface Knudsen number for one of the ports in the windward/leeward pressure pair rises above approximately 0.1, that pair is no longer usable. Although it is conceivable that a calibration for rarefied flow-induced dc pressure offsets could be developed, the best approach is to design the RFADS system to be insensitive to the induced pressure errors. The engineering model presented in this paper should prove acceptably accurate for preliminary designs or for a first-order engineering analysis.

References

[1] Berg, H., and Tijdeman, H., "Theoretical and Experimental Results for the Dynamic Response of Pressure Measuring Systems," Nat. Luchtavaatlab NLR-TR F.238, Amsterdam, Jan. 1965.

[2] Von Knudsen, M., "Eine Revision der Gleichgewichtsbedingung der Gase: Thermische Molekularstrmung," *Annalen der Physik (Berlin)*, Vol. 31, Nov. 1910, pp. 205–229.

[3] Kennard, E. H., *Kinetic Theory of Gases*, 1st ed., McGraw–Hill, New York, 1938, pp. 311–337.

[4] Maxwell, J. C., "On Stress in Rarefied Gases Arising from Inequalities of Temperature," *Philosophical Transactions of the Royal Society B*, Vol. 170, Pt. 1, London, England, U.K., Jan. 1879, pp. 231–235.

[5] Tompkins, J., and Wheeler, L., "The Correction for Thermo-Molecular Flow," *Transactions of the Faraday Society*, Vol. 29, No. 140, Nov. 1933, pp. 1248–1254. doi:10.1039/tf9332901248

[6] Whitmore, S. A., Petersen, B. J., and Scott, D. D., "A Dynamic Response Model for Pressure Sensors in Continuum and High Knudsen Number Flows with Large Temperature Gradients," NASA TM 4728, Jan. 1996.

[7] Whitmore, S. A., "Frequency Response of Pressure Sensor Configurations in Slip-Flow Conditions," *Journal of Spacecraft and Rockets*, Vol. 39, No. 2, March–April 2002, pp. 219–226.

[8] Rade, L., and Westergren, B., *Beta Mathematics Handbook*, 2nd ed., CRC Press, Boca Raton, FL 1990, pp. 287–288.

[9] Holman, J. P., *Experimental Methods for Engineers*, 3rd ed., McGraw–Hill, New York, 1978, pp. 280–282.

[10] Wright M. J., "Aerothermal Modeling for Entry and Aerocapture," Paper D9P1-NSTC-07-0026, 2007.

[11] Munk, M., M., "Aerocapture Technology Developments from NASA's In-Space Propulsion Technology Program," Paper D8P1-NSTC-07-0125, 2007.

[12] Greathouse, J. S., Kirk, B. S., Lillard, R. P., Truong, T. H., Robinson, P., and Cerimele, C. J., "Crew Exploration Vehicle (CEV) Crew Module Shape Selection Analysis and CEV Aeroscience Project Overview," *45th AIAA Aerospace Sciences Meeting and Exhibit*, AIAA Paper 2007-603, Jan. 2007.

[13] Anderson, B. M., and Whitmore, S. A., "Aerodynamic Control on a Lunar Return Capsule Using Trim-Flaps," *45th AIAA Aerospace Sciences Meeting and Exhibit*, AIAA Paper 2007-1200, Jan. 2007.

[14] While, D. M., "Shuttle Entry Air Data System Hardware Development," NASA CR-166044, 1983.

[15] Sutherland, W., "The Viscosity of Gases and Molecular Force," *Philosophical Magazine*, Vol. 5, No. 36, 1893 pp. 507–531.

I. Boyd
Associate Editor